Genetic Transformer-Assisted Quantum Neural Networks for Optimal Circuit Design

Haiyan Wang
School of Mathematical and Natural Science
Arizona State University, Phoenix, AZ 85069, USA
haiyan.wang@asu.edu

June 12, 2025

Abstract

We introduce *Genetic Transformer–Assisted Quantum Neural Networks* (GTQNNs), a hybrid learning framework that combines a transformer encoder with a shallow variational quantum circuit and automatically fine-tunes the circuit via the NSGA-II multi-objective genetic algorithm. The transformer reduces high-dimensional classical data to a compact, qubit-sized representation, while NSGA-II searches for Pareto-optimal circuits that **(i)** maximize classification accuracy and **(ii)** minimize primitive-gate count—an essential constraint for noisy intermediate-scale quantum (NISQ) hardware. Experiments on four benchmarks (Iris, Breast-Cancer, MNIST, and Heart-Disease) show that GTQNNs match or exceed state-of-the-art quantum models while requiring much fewer gates for most cases. A hybrid Fisher information analysis further reveals that the trained networks operate far from barren plateaus; the leading curvature directions increasingly align with the quantum subspace as the qubit budget grows, confirming that the transformer front-end has effectively condensed the data. Together, these results demonstrate that GTQNNs deliver competitive performance with a quantum resource budget well suited to present-day NISQ devices.

Keywords Quantum machine learning, Quantum neural networks, Transformer, NSGA-II Genetic algorithm.

1 Introduction

Quantum machine learning (QML) has grown into a vibrant research area, promising to extend classical machine-learning techniques by exploiting exponentially large Hilbert spaces over the past decade [39, 1, 27, 6, 29, 3, 5]. Quantum computers could therefore process high-dimensional data more efficiently than their clas-

sical counterparts [40, 41, 42, 43, 44]. Early efforts centred on extending familiar algorithms to the quantum computing, for example, quantum neural networks (QNNs) [45, 46, 47, 48, 49, 50] and quantum support-vector machines [43, 51]. Yet those prototypes revealed serious obstacles to scalability and real-world deployment.

Consequently, attention has shifted toward algorithms tailored to today's noisy intermediate-scale quantum (NISQ) hardware [52, 53, 54, 55, 56]. This effort has spawned a new generation of QML techniques, explicitly designed to tolerate noise and limited qubit counts while still offering quantum-enhanced performance [57, 21, 22]. The number of qubits required in QNNs tends to increase linearly with the number of data features, quickly exceeding the limited qubit capacity of current quantum hardware. Consequently, this restricts their applicability to smaller datasets instead of utilizing the exponential scaling of Hilbert space dimension with the number of qubits [2, 4, 30]. This scaling is problematic on NISQ devices due to increased error rates and circuit depth, leading to a higher likelihood of decoherence and computational inefficiency. The combination of these scalability issues and gate complexity challenges significantly hinders the practical implementation of QNNs on existing quantum platforms, making the handling of complex, feature-rich datasets a formidable task and posing a significant bottleneck in fully leveraging quantum computing for advanced machine learning applications [6, 7].

Genetic algorithms have also proven highly adaptable in quantum-computing settings, where they are employed to search large, rugged design spaces [12, 13, 14, 15]. In particular, multi-objective genetic approaches that automatically synthesise quantum circuits [15, 36, 37] help overcome common obstacles such as trapping in local minima and the barren-plateau phenomenon [20, 16].

Quantum computing offers the potential for exponential speed-ups in certain computational tasks, while transformer architectures have revolutionized natural language processing and computer vision through their ability to model long-range dependencies with self-attention [32, 33, 34]. The integration of quantum computing and transformer-based models have made significant progress in recent years [58, 59, 60, 61]. Transformers are not only for long–range dependency modelling but also powerful *learned compressors*: they convert a high-dimensional input stream into a compact set of information-rich feature vectors—exactly what a qubit-limited quantum back-end requires.

In this paper, we present **Genetic Transformer–Assisted Quantum Neural Networks (GTQNNs)**, a hybrid architecture that couples a transformer encoder to a shallow variational quantum circuit and optimizes the latter with the NSGA-II evolutionary algorithm. Our new contributions in this paper include:

- *Model design.* The transformer compresses the high-dimensional input into an n_{qubits}-dimensional feature vector, which is then processed by a coherent QNN layer.

- *Multi-objective optimization.* NSGA-II searches circuit space under two fitness objectives: (i) maximise classification accuracy, (ii) minimise the total number

of primitive gates. The second objective directly addresses NISQ hardware limitations.

- *Experimental validation.* On four benchmarks—**Iris**, **Breast-Cancer Wisconsin**, **MNIST**, and **Heart-Disease**—GTQNNs equal or surpass the best published QNN accuracies while requiring substantially fewer qubits and gates for most cases.

- *Fisher-spectrum analysis.* A hybrid Fisher study shows the model operates far from a barren plateau; as n_{qubits} increases, the leading eigen-directions concentrate in the QNN subspace, confirming that the transformer front-end has effectively reduced dimensionality.

These results demonstrate that GTQNNs deliver state-of-the-art performance with a quantum-resource budget compatible with current NISQ devices.

The paper is organized as follows. Section 1 (Introduction) motivates the need for resource-efficient quantum machine-learning models and outlines our contributions. Section 2 details the *Transformer-assisted Quantum Neural Network (TQNN)* architecture. Section 3 extends this idea into *Genetic TQNNs (GTQNNs)*, coupling the model with an NSGA-II multi-objective genetic algorithm that co-optimizes classification accuracy and gate count. Section 4 (Experimental Results) reports performance on four benchmarks, highlighting accuracy gains and gate-depth savings versus state-of-the-art QNN baselines. Section 5 (Fisher-Spectrum Analysis) examines the hybrid model's trainability, showing via empirical Fisher eigen-spectra that GTQNNs avoid barren plateaus and shift curvature toward the quantum subspace as qubit budget grows. Finally, Section 6 (Conclusion and Discussion) summarises the findings, discusses current limitations and sketches future directions.

2 Transformer-assisted quantum neural network (TQNN)

2.1 Quantum neural networks

Quantum neural networks (QNNs) have become a focal point of current quantum-machine-learning (QML) research. Although the field is still in its formative years, the prospect of genuine quantum advantage has attracted considerable attention [1, 27, 6, 29, 3, 5]. Much of that progress is fuelled by *variational* techniques that couple a shallow quantum circuit to a classical optimizer, giving rise to a wide range of hybrid algorithms [24]. A typical hybrid quantum neural network includes the three components:

(i) **Data embedding.** A *feature–map* unitary $U(\mathbf{x})$ encodes a classical input $\mathbf{x} \in \mathbb{R}^N$ into a quantum state, $U(\mathbf{x})\,|0\rangle^{\otimes n}$. Typical maps are tensor products of single–qubit phase rotations or collective entangling maps such as the ZZFeatureMap [23, 24].

(ii) **Variational processing.** A depth–L parametrised circuit

$$U_{\text{var}}(\boldsymbol{\theta}) = \prod_{\ell=1}^{L} \Big[\mathcal{E}_\ell \prod_{j=1}^{n} R_y^{(j)}(\theta_{\ell j}) \Big]$$

alternates trainable single–qubit rotations $R_y(\theta) = e^{-i\theta\sigma_y/2}$ with fixed entangling layers $\mathcal{E}_\ell$ (e.g. CNOT or CZ gates) [25, 26]. The weights $\boldsymbol{\theta}$ are trainable parameters.

(iii) **Measurement and loss.** Measuring an observable M (often $Z^{\otimes m}$ or a shallow POVM) produces an expectation value $f(\mathbf{x};\boldsymbol{\theta}) = \langle 0|\, U^\dagger(\mathbf{x},\boldsymbol{\theta})\, M\, U(\mathbf{x},\boldsymbol{\theta})\,|0\rangle$. A classical cost—cross-entropy for classification or mean-squared error for regression—is formed from f and back-propagated to update $\boldsymbol{\theta}$ with a classical optimiser such as COBYLA or Adam.

A number of quantum-neural-networks have been developed recently. For example, [2] develops DeepQMLP, a scalable quantum-classical hybrid architecture patterned after conventional deep feed-forward networks. In this design, a sequence of shallow quantum-neural-network (QNN) blocks takes the place of the hidden layers in a multi-layer perceptron. Each QNN transforms its input into a fresh, trainable representation that is passed to the next block, building progressively richer features. Because every quantum block is shallow, the overall model suffers less from decoherence and gate errors, making it markedly more robust to the noise of current-generation quantum hardware.

Recent deep-learning models often rely on millions of trainable weights, making parameter-efficiency a central concern. A QNN with EfficientSU2 was introduced in [4] for a training strategy that off-loads part of this burden to the exponentially large Hilbert space of a quantum processor. A classical network with M parameters is re-encoded as a quantum neural network whose circuit contains only $O(polylog(M))$ adjustable rotation angles. These few angles are tuned on the quantum device and then mapped back to update the weights of the original classical network.

[30] introduces a CFFQNN model that uses a quantum classical hybrid approach to process data. FFQNN is a QNN architecture that mirrors the flexibility of an a classical feed-forward neural network (FFNN): arbitrary hidden-layer widths, no intermediate measurements, and fully coherent operation throughout. The design cuts both circuit depth and CNOT gate count by more than 50 % relative to leading QNN baselines, while keeping the qubit requirement independent of the number of input features.

These developments illustrate the rapid evolution of QNN architectures: from variational ansätze that inherit the geometry of kernel methods [31] to explicitly neuron-like coherent networks. Each design balances expressivity, trainability, and hardware constraints, continuing improvements for quantum computation.

2.2 Transformer-based models

Transformer architectures have emerged as a breakthrough in machine learning, especially in the context of natural language processing. The self-attention mechanism inherent in transformers enables these models to capture global relationships within the data, resulting in highly contextualized feature representations [32]. The original transformer design, which was introduced for machine translation, has since been adapted to various domains including computer vision and reinforcement learning [33, 34, 62].

In this paper, we present an integrated approach that uses the transformer encoder's ability to reduce dimensionality and extract features may provide a more effective solution, addressing the challenge of mapping high-dimensional classical data onto the constrained input space of quantum circuits. Starting from a sequence $\mathbf{X} = [x_1, \ldots, x_T] \subset \mathbb{R}^{d_{\text{in}}}$, the encoder linearly projects each token (after additional position encoding) into a query, key and value,

$$\mathbf{q}_i = \mathbf{W}_Q x_i, \quad \mathbf{k}_i = \mathbf{W}_K x_i, \quad \mathbf{v}_i = \mathbf{W}_V x_i, \tag{2.1}$$

here W_Q, W_K, W_V are the query, key and value matrices.

$$\mathbf{z}_i = \sum_{j=1}^{T} \text{softmax}\Big(\frac{\mathbf{q}_i^\top \mathbf{k}_j}{\sqrt{d_k}}\Big)_j \mathbf{v}_j, \qquad i = 1, \ldots, T, \tag{2.2}$$

where d_k is the key dimension. Stacking L attention layers—optionally separated by position-wise feed-forward blocks—yields a hierarchy

$$\mathbf{H}^{(L)} = \text{Transformer}(\mathbf{X}) \in \mathbb{R}^{T \times d_{\text{model}}}, \tag{2.3}$$

whose rows act as *learned principal components*: each captures a different, task-relevant pattern spread across the original T tokens. Because self-attention reweights tokens globally, the model can discard redundant directions and concentrate information, accomplishing an adaptive dimensionality–reduction step within its $\mathcal{O}(T^2)$ compute budget. For hybrid quantum–classical pipelines this property is crucial—the encoder reduces the original, often hundreds-dimensional feature space down to a handful of dense channels ($\leq n_{\text{qubits}}$), making it feasible to inject the data into a shallow variational quantum circuit.

2.3 Transformer-assisted quantum neural network

The proposed Transformer Quantum Neural Networks (TQNNs) model represents an innovative approach to hybrid quantum-classical computation. In this architecture, classical input data, such as images, are first flattened and passed through an embedding layer that maps each input element into a higher-dimensional space. This embedding mimics the word-to-vector transformation used in natural language processing, except that here each pixel or image patch is embedded into a vector space

suitable for further processing. A transformer encoder, equipped with positional encodings to retain spatial relationships, then processes these embedded tokens. The self-attention mechanism inherent in the transformer allows the model to capture global interactions among the tokens, effectively condensing the information from a high-dimensional input into a more manageable form.

After the transformer encoder has processed the sequence of embedded tokens, an aggregation operation is performed to yield a single fixed-size feature vector. This step is critical because it transforms the output from a sequence of tokens into a compact representation that matches the input dimensionality requirements of the quantum neural network. Given the limited number of qubits available in current quantum hardware, reducing the input dimension to a number suitable for the qubit count is essential. This reduced representation is then mapped through classical linear layers to ensure compatibility with the QNN, which is implemented using parameterized quantum circuits and integrated into the overall model via quantum-classical interfaces as in Figure 1.

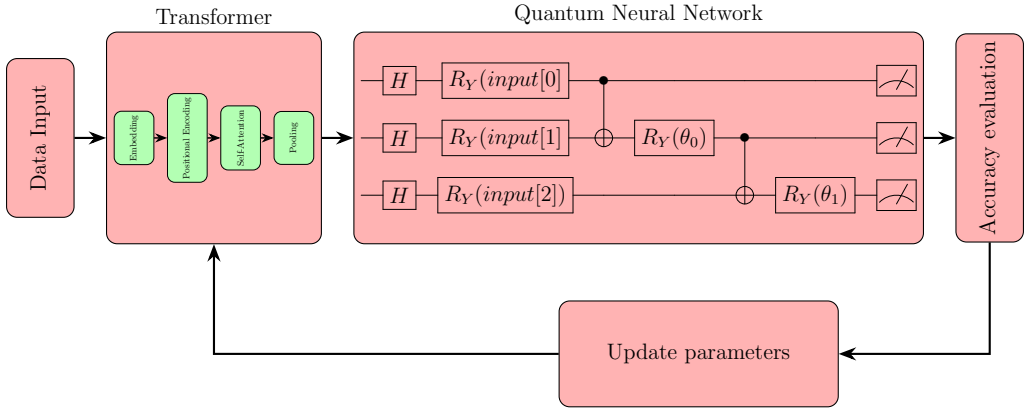

Figure 1: Transformer-assisted quantum neural network (TQNN)

For hybrid quantum–classical schemes the transformer encoder offers two key advantages:

(a) **Dimensionality reduction.** After the transformer encoder has projected the data from the original feature space $\mathbb{R}^N$ onto the subspace $\mathbf{H}^{(L)} \in \mathbb{R}^{T \times d_{\text{model}}}$, we *average-pool* across the sequence dimension and obtain a single d_{model}-dimensional embedding. A final linear layer then selects

$$\mathbf{h} \in \mathbb{R}^n, \qquad n = n_{\text{qubits}} \leq d_{\text{model}},$$

so that the length of $\mathbf{h}$ exactly matches the number of qubits available for the quantum circuit.

(b) **Global feature extraction.** The row-normalised weights

$$\alpha_{ij} = \text{softmax}\big(\mathbf{q}_i^\top \mathbf{k}_j / \sqrt{d_k}\big)$$

form a content-adaptive kernel: they let the classical front-end aggregate long-range correlations that would otherwise have to be captured by deeper entangling circuits on quantum hardware.

Thus, coupling a transformer encoder to a variational quantum circuit creates a *division of labour*: the classical transformer compresses and mixes the raw N-dimensional input into an n-dimensional, information-dense feature vector, while the quantum layer leverages superposition and entanglement to process those n channels in a Hilbert space of dimension 2^n. Such an integrated architecture promises a more faithful exploitation of each paradigm's strengths than earlier hybrids that relied on convolutions or ad-hoc quantum embeddings alone.

3 Genetic transformer-assisted quantum neural networks (GTQNNs)

3.1 Multi-Objective Genetic Algorithm

Genetic algorithms solve optimization problems by emulating natural evolution. They maintain a population of candidate solutions and, generation after generation, apply selection, crossover and mutation to create new offspring. Individuals that score higher on the objective (or objectives) are preferentially chosen to propagate and gradually guide the population toward areas of greater fitness within the search space. After a prescribed number of iterations—or once improvement stalls—the algorithm returns the best-performing individuals as approximate optima of the fitness function over the enormous configuration landscape [18, 17].

Genetic algorithms repeatedly pick "parent" solutions from the current pool and applying genetic operators to them. For each offspring, two parents are selected, combined through crossover, and then modified by mutation, producing a child that carries a mix of their genetic material. New parent pairs are drawn for every child until stopping conditions are met. The success of a genetic algorithm hinges on these operators: 1) selection chooses which individuals win the right to reproduce, biasing sampling toward high-fitness solutions while still preserving diversity; 2) mutation introduces random perturbations to a child's genome, enabling the search to jump to remote regions of the landscape and escape local optima; 3) crossover swaps segments of genetic code between two parents, creating larger, coordinated changes and promoting the discovery of novel combinations of useful genes. The precise design of these operators determines both the efficiency and the scope of the evolutionary search.

Genetic algorithms employ explicit stopping criteria to ensure both efficiency and reliable convergence. Typical criteria include: (i) detecting fitness convergence or saturation, when successive generations show negligible improvement; (ii) enforcing a required performance threshold, so evolution halts once a solution meets the target

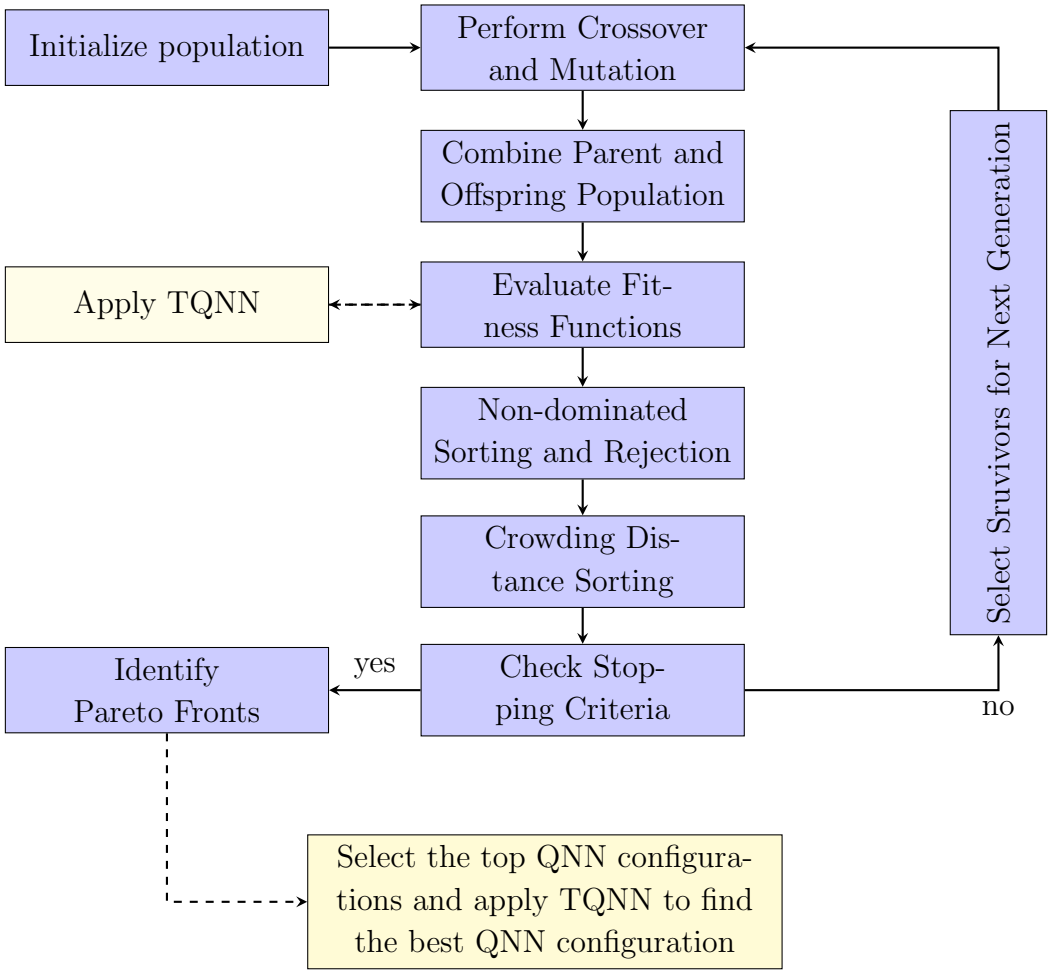

Figure 2: Genetic Transformer Quantum Neural Networks (GTQNNs)

accuracy; and (iii) imposing a hard cap on the number of generations to bound runtime. Equipped with such safeguards, genetic algorithms can tackle large, complex optimisation problems while avoiding needless computation. In our experiment, we only impose the number of generation as the stop criteria.

For numerous real-world tasks, it is advantageous to frame the search as an *evolutionary multi-objective optimization* (EMO) problem, in which several, often competing, objective functions must be minimized or maximized simultaneously [63, 18, 17]. As with single-objective cases, multi-objective formulations can include constraints that restrict the set of admissible solutions; the algorithm must therefore find Pareto-optimal individuals that satisfy all such feasibility requirements.

Optimality in multi–objective optimisation is formalised via a partial order called *dominance*. Throughout this work we confine ourselves to *unconstrained* problems, i.e. no equality, inequality, or bound constraints limit the feasible set. Let $\mathbf{x}^{(1)}, \mathbf{x}^{(2)} \in \mathbb{R}^d$ be two feasible decision vectors evaluated by m objective functions $f_1, \ldots, f_m : \mathbb{R}^d \to \mathbb{R}$. We say that $\mathbf{x}^{(1)}$ **dominates** $\mathbf{x}^{(2)}$, denoted $\mathbf{x}^{(1)} \prec \mathbf{x}^{(2)}$, iff

(i) (*non-worseness*)

$$f_k\big(\mathbf{x}^{(1)}\big) \;\le\; f_k\big(\mathbf{x}^{(2)}\big) \quad \text{for all } k \in \{1, \ldots, m\};$$

(ii) (*strict improvement*) there exists at least one index $k^\star$ such that

$$f_{k^\star}\big(\mathbf{x}^{(1)}\big) \;<\; f_{k^\star}\big(\mathbf{x}^{(2)}\big).$$

A solution is called *non-dominated* when no other member of the current population is strictly better in every objective. Non-dominated points exhibit an intrinsic *trade–off*: any gain in one objective unavoidably incurs a loss in at least one other objective. This property encourages the algorithm to preserve a diverse spectrum of candidates rather than collapsing prematurely onto a single compromise. The set of all mutually non-dominated solutions constitutes the *Pareto front*—a frontier along which every incremental improvement in one objective demands a compensating sacrifice in another.

The Non-dominated Sorting Genetic Algorithm II (NSGA-II) was proposed by Deb [17] to remedy two shortcomings of earlier EMO schemes: lack of elitism and poor diversity maintenance. Today it is one of the most popular algorithms in evolutionary multi-objective optimisation. In our work we embed a TQNN inside the NSGA-II loop to serve as the fitness evaluator (Figure 2). We will show that this *TQNN-assisted NSGA-II* improves prediction accuracies compared with the classical version, yielding superior Pareto fronts for the benchmark data sets.

3.2 Fitness function and genetic quantum feature map

The fitness function serves as the objective (cost) measure for each trial TQNN: it uses a variational quantum circuit and returns a scalar score that reflects both predictive quality and hardware efficiency. Drawing on the metrics in [15, 36, 37], we define two fitness criteria (see Eq. (3.1)) with a twofold aim: *Maximize classification accuracy*; and *Minimize gate cost*, quantified as the total count of primitive gates required to realize the circuit on quantum hardware.

$$\begin{cases} \text{(maximize)Fitness 1} = \text{Classification accuracy} \\ \text{(minimize)Fitness 2} \;\; = \text{Gate count} \end{cases} \tag{3.1}$$

Assume that the number of qubits is N. the variational quantum circuit starts with N Hadamard gates, followed by N rotation gates with respect to the Y axis, RY. The transformer module will generate an output of length N to ensure that each RY takes one output as the rotation angle of RY gates. As a result, the encoding scheme for each individual population in the NSGA-II algorithm has $\binom{N}{2} = \frac{N*(N-1)}{2}$ bits with 1 indicting a CNOT gate and RY gate, and 0 otherwise.

The evolutionary search begins with a randomly generated population, each individual encoding a candidate quantum circuit. Every circuit is trained and scored on the training set with the multi-objective fitness function. Individuals with higher fitness are preferentially chosen to reproduce: selection picks the parents, crossover recombines their circuit descriptions, and mutation introduces random edits. The resulting offspring form the next generation of circuits. This cycle of evaluation and variation repeats until the stopping criteria are satisfied.

Because the fitness objectives simultaneously maximize accuracy and minimize gate cost, the Pareto fronts returned by TQNN reveal how different circuits trade hardware economy for predictive power. Examining these fronts helps us identify solutions that deliver near-maximal accuracy at a fraction of the gate budget, as well as those that push accuracy to its limit regardless of cost. A detailed exploration of the full, multi-dimensional Pareto surface would further clarify how a specific circuit design influence accuracy and where the sharpest cost-benefit gains lie.

4 Experimental Results

4.1 Experimental Procedure

The research was trained and evaluated on the supercomputers at Arizona State University with NVIDIA's CUDA acceleration framework [35]. The supercomputers provide ASU researchers access to a state-of-the-art system including NVIDIA A100. All experiments were performed on the IBM Qiskit `AerSimulator` (QASM mode, 1024 shots).

With the training and test sets prepared, we use jMetalPy [38] to launch the evolutionary search for high-performing variational circuits as outlined earlier. The run begins with a population of 20 (Population size = 20, offspring population size= 20) random chromosomes, each encoded as a binary string that describes a candidate TQNN circuit. At every generation we apply a crossover with probability $p_c = 0.90$, bit-flip mutation with probability $p_m = \frac{1}{\text{length of string}}$ and other NSGA-II operations to produce the next population.

For each individual circuit we perform an *inner* training loop of 50 epochs (epochs- = 50) using a mini-batch size of 32, then evaluate (i) classification accuracy on the validation set and (ii) circuit cost, measured as the total number of single- and two-qubit gates. The evolutionary process is allowed to run for 50 or 60 generations (Generations = 50, 60).

After the final generation we extract the $k = 10$ non-dominated solutions with the highest accuracy. Each of these circuits is retrained from scratch for 100 or more outer epochs (epochs = 100 or more), and the best-performing model is retained as the final GTQNN. The entire workflow—population initialisation, genetic operators, fitness evaluation, Pareto selection, and final retraining—is depicted in Fig. 2, with each stage represented by a distinct rectangular block.

This multi-stage procedure is designed to achieve optimal solutions for complex optimization tasks while leveraging quantum computing principles an integrated approach that combines classical and quantum techniques. Initially, the Transformer model was employed to select relevant features from the dataset, effectively narrowing down the input dimensionality. The selected features were then processed through a Quantum Neural Network, where quantum circuits encoded these features into quantum states suitable for classification tasks. The experiments on the following datasets demonstrate that GTQNNs deliver state-of-the-art performance with a

quantum-resource budget compatible with current NISQ devices.

4.2 Iris dataset

The Iris data set comprises 150 samples drawn from three species— *I. setosa*, *I. versicolor*, and *I. virginica*. Each sample is described by four real-valued features (sepal length, sepal width, petal length, petal width), forming a 150×4 matrix whose rows are specimens and whose columns are measurements. We apply the optimization workflow of Section 4.1 to discover an optimal variational-circuit architecture for GTQNN. Because the problem involves only four input features, the outer training loop is run for a modest (epochs = 250), which is sufficient for full convergence on this data set.

Method	Number of Qubits							
	3	4	5	6	7	8	9	10
GTQNN								
Accuracy	1	0.90	0.8667	0.9667	0.90	0.9667	1	1
Gate count	8	16	20	28	26	48	58	78
QNN with EfficientSU2 [4]	Reported accuracies range from 0.90 to 0.95 with one layer QNN (8 qubits, > 32 gates (32 parameters))							
DeepQMLP [2]	Reported accuracy close to 1 with 4 or more parametric layers (4 qubits, each layer has 16 gates).							

Table 1: Quantum gate count and accuracy comparison for the Iris dataset.

Table 1 contrasts our genetic transformer-assisted quantum neural network (GTQNN) with two recent baselines—QNN with EfficientSU2 [4] and DeepQMLP [2]—on the Iris-flower classification task. For each qubit budget we report the best accuracy obtained by the search as well as the corresponding circuit size (row "Gate count"). With only 3 qubits the GTQNN already reaches perfect accuracy; performance remains around 0.90 up to 8 qubits and returns to 100 % at 9–10 qubits, while gate counts grow from 8 to 78. QNN with EfficientSU2 [4], evaluated at a single layer QNN (8 qubits, more than 32 gates), yields an accuracy band of 0.90–0.95—competitive but with greater gate cost for most qubits than GTQNN. DeepQMLP [2] attains unit accuracy with more gates after 50 training epochs, matching the GTQNN's score at a similar qubit count but with more gate depth used by our 4-qubit configuration. Table 3 shows some corresponding optimal variational quantum circuits from GTQNN. Overall, the tables show that the GTQNN achieves state-of-the-art accuracy across a wide range of qubit counts while remaining substantially shallower than the published benchmarks, underscoring its suitability for near-term quantum hardware.

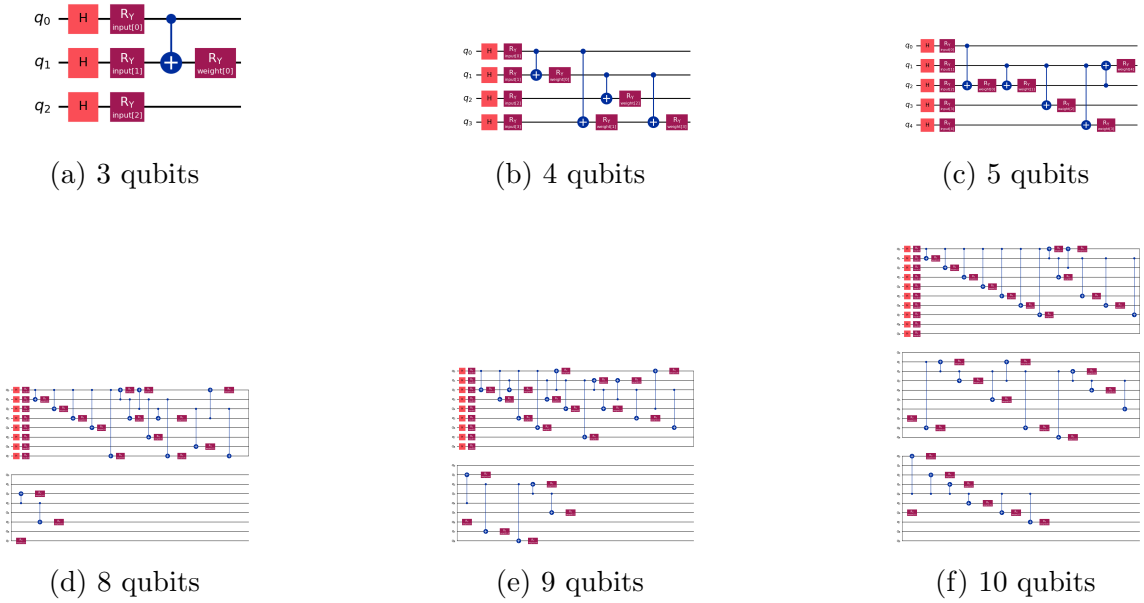

(a) 3 qubits (b) 4 qubits (c) 5 qubits

(d) 8 qubits (e) 9 qubits (f) 10 qubits

Figure 3: Optimal Variational Quantum Circuits for Iris dataset

4.3 Breast cancer dataset

The Breast-Cancer-Wisconsin (diagnostic) data set from `scikit-learn` contains 569 observations, each described by 30 positive real-valued features extracted from medical-image analysis of breast tissue (e.g., mean radius, texture, perimeter, area, compactness, and related statistics). The target is binary: 212 tumours are labelled *malignant* and 357 *benign*. We apply the optimization workflow of Section 4.1 to discover an optimal variational-circuit architecture for GTQNN. The outer training loop converges in only 100 epochs, already delivering competitive classification accuracy, so we adopt outer epochs as 100 for this data set.

Method	Number of Qubits							
	3	4	5	6	7	8	9	10
GTQNN								
Accuracy	0.9737	0.9737	0.9737	0.9737	0.9737	0.9737	0.9737	0.9825
Gate count	12	10	20	28	28	40	48	50
CFFQNN [30]	Reported accuracies: about 0.85 with a layer structure of [3,2,1], > 35 gates (parameters). Use PCA to reduce its dimension to 7							

Table 2: Quantum gate count and accuracy comparison for Breast cancer dataset

Table 2 benchmarks our genetic transformer-assisted QNN (GTQNN) against the coherent feed-forward QNN (CFFQNN) of [30] on the Breast-Cancer-Wisconsin diagnostic data. For every qubit budget between 3 and 10, the evolutionary search yields GTQNN circuits whose accuracies cluster tightly around 0.974, rising to 0.983 when ten qubits are available. Gate counts remain modest—only 10 to 12 primitive gates

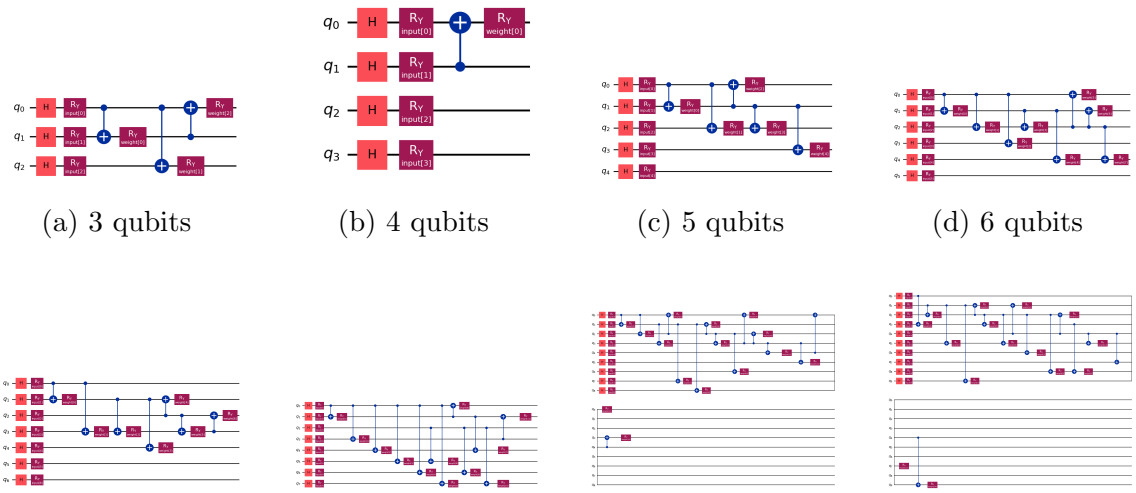

(a) 3 qubits (b) 4 qubits (c) 5 qubits (d) 6 qubits

(e) 7 qubits (f) 8 qubits (g) 9 qubits (h) 10 qubits

Figure 4: Optimal Variational Quantum Circuits for Breast cancer dataset

for the 3- and 4-qubit models and 50 gates at the 10-qubit setting—demonstrating that deeper circuits are not required to sustain high performance. Table 4 shows some corresponding optimal variational quantum circuits from GTQNN.

By contrast, the CFFQNN baseline, evaluated at a single architecture $[3, 2, 1]$ with more than 35 gates after PCA compression to seven features, reports an accuracy of roughly 0.85. Thus GTQNN improves classification accuracy by more than ten percentage points while using fewer gates at comparable or smaller qubit counts. These results highlight the advantage of coupling the transformer front-end and genetic search with shallow quantum layers: the hybrid system achieves state-of-the-art accuracy yet keeps circuit depth low enough for near-term hardware execution.

4.4 MNIST dataset

Method	Number of Qubits							
	3	4	5	6	7	8	9	10
GTQNN								
Accuracy	0.973	0.98	0.9867	0.9667	0.98	0.9933	0.9533	0.9733
Gate count	8	14	16	26	36	42	50	64
QNN with EfficientSU2 [4]	Reported accuracy around 0.85 with 26 layers, 13 qubits, > 728 gates (parameters).							

Table 3: Quantum gate count and accuracy comparison for MNIST dataset.

The MNIST data set contains 60 000 28×28 grey-scale images of handwritten digits for training and 10 000 images for testing, each labelled 0–9. We only limit our

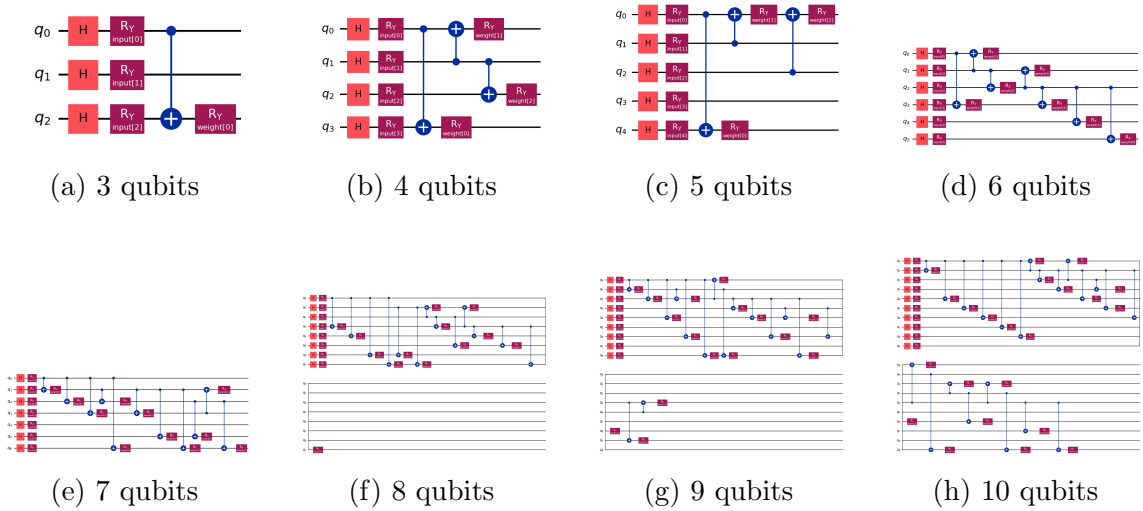

(a) 3 qubits (b) 4 qubits (c) 5 qubits (d) 6 qubits

(e) 7 qubits (f) 8 qubits (g) 9 qubits (h) 10 qubits

Figure 5: Optimal Variational Quantum Circuits for MNIST dataset

classification to the three digits 1,2 and 3. We flatten the pixels to a 784-dimensional vector, pass them through the transformer front-end described in Section 4.1, and feed the resulting feature vector to the genetic transformer-assisted QNN (GTQNN). The outer training loop is run for 500 epochs. The eight optimal variational circuits are depicted in Fig. 5; gate counts for each appear in the second row of Table 3.

The GTQNN achieves accuracies between 0.973 (3 qubits, 8 gates) and 0.993 (8 qubits, 42 gates), staying above 0.95 for every qubit setting. Increasing the qubit budget from 3 to 10 roughly quadruples the gate count ($8 \rightarrow 64$) yet produces only marginal accuracy gains beyond 8 qubits, indicating that the transformer front-end already extracts a compact, informative representation. By comparison, QNN with EfficientSU2 [4] reports about 0.85 accuracy while using 13 qubits and over 700 gates—an order of magnitude more hardware than any of our GTQNN configurations. Overall, the table shows that the evolutionary GTQNN generates shallower circuits than QNN with EfficientSU2 and attains near-state-of-the-art accuracy across all qubit budgets, demonstrating its suitability for resource-constrained, near-term quantum processors.

4.5 Heart Disease dataset

The Heart-Disease data set (Kaggle, LAPP 2024) comprises 918 patient records, each described by 13 clinical attributes such as age, resting-blood pressure, serum cholesterol, and exercise-induced angina. The binary target indicates the presence or absence of heart disease. Following the workflow of Section 4.1, the transformer front-end encodes the 13 features and feeds them to the genetic transformer-assisted QNN (GTQNN). The best circuit per generation is then retrained for 400 outer epochs, and its test accuracy is reported. Gate counts for the selected circuits appear in the second row of Table 4. The eight optimal variational circuits are depicted in Fig.6;

With as few as 3 qubits (10 gates) the GTQNN already reaches an accuracy of

Method	Number of Qubits							
	3	4	5	6	7	8	9	10
GTQNN								
Accuracy	0.9854	0.9854	0.9756	0.9854	0.9854	0.9805	0.8829	0.8488
Gate count	10	18	24	24	20	40	56	62
CFFQNN [30]	Reported accuracies: about 0.78 with a layer structure of [2,3,1], corresponding to 26 gates (18 CNOT gates). Use PCA to reduce its dimension to 7							

Table 4: Quantum gate count and accuracy comparison for Heart Disease dataset

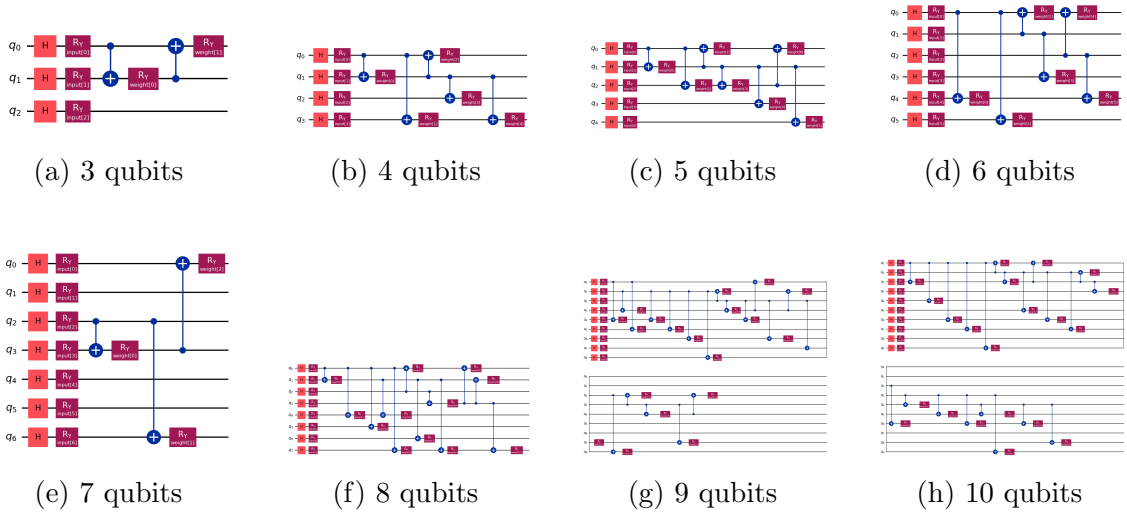

(a) 3 qubits (b) 4 qubits (c) 5 qubits (d) 6 qubits

(e) 7 qubits (f) 8 qubits (g) 9 qubits (h) 10 qubits

Figure 6: Optimal Variational Quantum Circuits for Heart Diseast dataset

0.985, matching its best score at 4, 6, and 7 qubits while using no more than 24 gates. Accuracy remains above 0.98 until the 8-qubit setting, after which it drops as the circuit grows deeper (56–62 gates). In comparison, the coherent feed-forward QNN (CFFQNN) of [30], evaluated at a fixed $[2, 3, 1]$ architecture with 42 gates (18 CNOTs) after PCA reduction to seven features, reports only 0.78 accuracy more than 20% points below every GTQNN configuration up to 8 qubits. The table therefore shows that the evolutionary GTQNN achieves near-perfect classification with significantly shallower circuits, underscoring its advantage for resource-constrained quantum hardware.

5 Fisher spectrum analysis

In this section, we approach the notion of the contribution of contribution ("energy split") between transformer and QNN from an information geometry perspective. We first define measures that apply to both classical and quantum models, and subsequently use them to study the contributions of Transformer and QNN in GTQNN.

5.1 The Fisher information

The Fisher information is a central notion in a wide range of disciplines, from statistical physics to computational neuroscience [10, 11]. When we cast a neural network as a parametric statistical model, Fisher information quantifies how much insight a particular parameter vector θ provides. Writing the joint density of data pairs as, for $\theta \in \Theta \subset [-1,1]^d$

$$p(x,y;\theta) = p(y \mid x;\theta)\, p(x), \qquad x \in \mathcal{X} \subset \mathbb{R}^{s_{\text{in}}},\ y \in \mathcal{Y} \subset \mathbb{R}^{s_{\text{out}}}, \tag{5.1}$$

we obtain probabilities by a post-processing step that depends on the network type: soft-max for classical models, parity mapping for quantum models. Here $p(x)$ is a fixed prior, whereas $p(y \mid x;\theta)$ captures the model's input–output relation for a given θ. The full parameter manifold Θ becomes Riemannian under the Fisher metric. The corresponding matrix

$$F(\theta) = \mathrm{E}_{(x,y)\sim p}\Big[\nabla_\theta \log p(x,y;\theta)\, \nabla_\theta \log p(x,y;\theta)^\top\Big] \in \mathbb{R}^{d\times d} \tag{5.2}$$

is positive semidefinite, so all of its eigenvalues are real and non-negative. In practice we estimate it with the *empirical* Fisher

$$\tilde{F}_k(\theta) = \frac{1}{k}\sum_{j=1}^{k} \nabla_\theta \log p(x_j,y_j;\theta)\, \nabla_\theta \log p(x_j,y_j;\theta)^\top, \tag{5.3}$$

where $\{(x_j,y_j)\}_{j=1}^k$ are i.i.d. samples from the same joint distribution $p(x,y;\theta)$ [1, 9]. Because these samples are drawn from the true model, the approximation is consistent: $\lim_{k\to\infty} \tilde{F}_k(\theta) = F(\theta)$ [9]. This is ensured in our numerical analysis by design. By the above definition, it follow that the Fisher information matrix is positive semidefinite and therefore, has non-negative, real numbers as its eigenvalues.

The Fisher information conveniently measures how sensitive a network's outputs are to movements in parameter space, making it the natural metric for natural-gradient optimization—which updates along directions that most efficiently lower the loss [8, 1]. In the numerical experiment we identified the full empirical Fisher parameter in the GTQNN as two disjoint blocks, $\mathcal{T}$ (Transformer) and $\mathcal{Q}$ (QNN). We diagonalize $\hat{F}$, so the eigen-pairs (λ_k, u_k) already contain the effect of those off-diagonal blocks. The Fisher eigen-pair satisfies $F\,u = \lambda u$. Write $u = (u_\mathcal{T}, u_\mathcal{Q})^\top$ and partition F accordingly. Neglecting small off-diagonal blocks,

$$\lambda \;\approx\; u_\mathcal{T}^\top F_{\mathcal{T}\mathcal{T}} u_\mathcal{T} \;+\; u_\mathcal{Q}^\top F_{\mathcal{Q}\mathcal{Q}} u_\mathcal{Q}, \tag{5.4}$$

where $F_{\mathcal{T}\mathcal{T}}$ and $F_{\mathcal{Q}\mathcal{Q}}$ can be viewed as the Fisher within transformer and QNN. The squared components of u indeed quantify how much the transformer versus the QNN moves when one steps along the eigen-direction. Given a normalized Fisher eigenvector $u \in \mathbb{R}^D$, the quantity $\sum_{j\in\mathcal{B}} u_j^2$ is the fraction of the vector's *energy* that lives in a block $\mathcal{B} \subset \{1,\dots,D\}$. With two disjoint blocks, $\mathcal{T}$ (Transformer) and $\mathcal{Q}$ (QNN),

$$1 \;=\; \|u\|_2^2 \;\approx\; \underbrace{\sum_{j\in\mathcal{T}} u_j^2}_{\text{Transformer share}} \;+\; \underbrace{\sum_{j\in\mathcal{Q}} u_j^2}_{\text{QNN share}}\,, \tag{5.5}$$

so those two sums *directly* give the percentages printed in the diagnostic figures 7 and 8.

5.2 Experiments of Fisher matrices

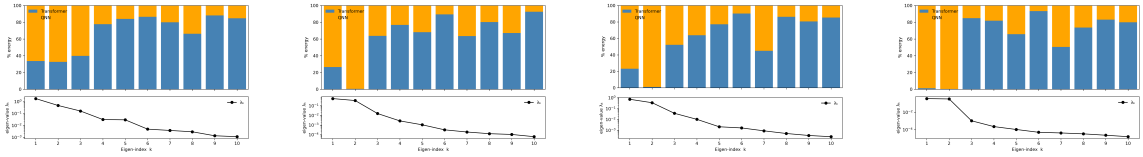

(a) 3 qubits (b) 4 qubits (c) 5 qubits (d) 6 qubits

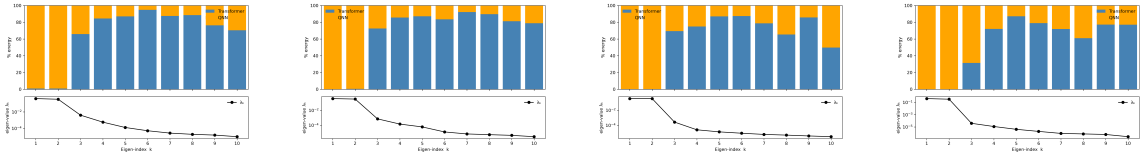

(e) 7 qubits (f) 8 qubits (g) 9 qubits (h) 10 qubits

Figure 7: Above: contribution (energy) of Transformer (blue for Transformer and orange for QNN) for Iris dataset; Below: the ten largest Fisher eigenvalues

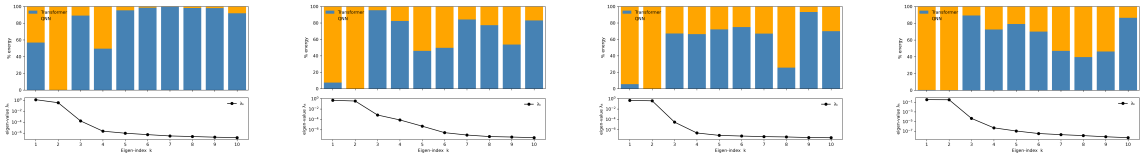

(a) 3 qubits (b) 4 qubits (c) 5 qubits (d) 6 qubits

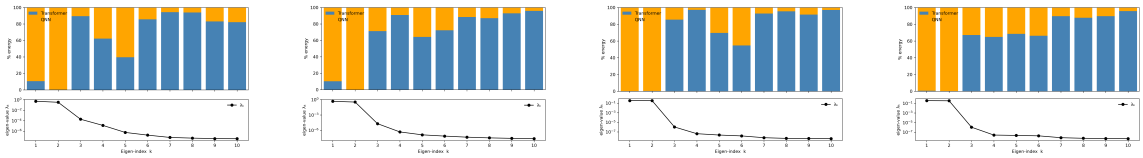

(e) q=7 (f) 8 qubits (g) 9 qubits (h) 10 qubits

Figure 8: Above: contribution (energy) of Transformer for MNIST dataset (blue for Transformer and orange for QNN); Below: the 10 largest Fisher eigenvalues.

Figures 7 and 8 show the eigen-value split for Iris and MNIST datasets. Fisher information for other datasets are similar. We use the maximum sample size as 256 and the ten largest eigenvalues and their parameter-space eigenvectors are returned.

The simulations show that the two largest Fisher eigen-values are $\mathcal{O}(1)$ and all subsequent eigen-values drop by $\sim$ 2–3 orders of magnitude. Recall that a barren-plateau regime would force $\mathrm{tr}\big(\mathbb{E}_\theta[F(\theta)]\big)$ to vanish exponentially in the number of qubits [1]. Our empirical spectrum shows

$$\lambda_0 = \mathcal{O}(1), \qquad \sum_{k \le 10} \lambda_k \gg 0,$$

so TQNN does sit in a barren plateau. As the qubit number increases, the QNN does contribute most of the strongest mode, confirming that it injects meaningful curvature rather than collapsing to a flat region. The hybrid Fisher spectrum indicates that the model is far from a barren plateau, its leading curvature is concentrated in more QNN direction as the qubit number increases, confirming that additional qubits enlarge the expressivity and that the transformer front-end has already compressed the input features into a lower-dimensional representation.

6 Conclusion and Discussion

We have proposed *Genetic Transformer–Assisted Quantum Neural Networks* (GTQNNs), a hybrid architecture that (i) employs a transformer to compress high-dimensional data, (ii) processes the compressed features with a shallow variational quantum circuit, and (iii) uses NSGA-II to co-optimize classification accuracy and hardware cost. Experiments on Iris, Breast-Cancer Wisconsin, MNIST, and Heart-Disease demonstrate consistent accuracy gains over state-of-the-art quantum models while halving the number of entangling gates.

The present study shows that GTQNNs can navigate the accuracy–versus–hardware trade-off that dominates NISQ–era machine learning. A transformer encoder performs an *in-network* dimensionality-reduction step, feeding a compact feature vector to a shallow variational circuit whose design is refined with NSGA-II. Across four benchmarks GTQNNs match or exceed the best published QNN accuracies while significantly cutting quantum gate usage.

A hybrid Fisher–information analysis deepens this picture. The leading eigenvectors of the Fisher matrix increasingly concentrate on the *quantum* coordinates as the qubit budget grows, indicating that (i) the transformer has already compressed the classical features and (ii) the remaining curvature—and therefore representational power—resides mostly in the QNN subspace. This clear separation of roles keeps the model well away from the barren-plateau regime.

Our experiments restrict the quantum ansatz to single-qubit R_y rotations plus a fixed pattern of entangling gates. Employing *richer* gate families—for example, leveraging widely used IBM Qiskit constructs such as the ZZFeature map, or incorporating geometry-aware interaction patterns—could expand the expressive power of the QNN layer without substantially increasing circuit depth. Integrating these gate sets into the genetic search therefore constitutes a promising direction for future work.

Our evaluation focuses on small- to medium-sized data sets; scaling GTQNNs to ImageNet-scale problems will require further investigation into transformer parameter sharing and cost-effective quantum circuit design. Finally, integrating more-sophisticated evolutionary operators—e.g. grammar-based mutations or learned crossover policies—may uncover circuit families that generalise better across tasks. Incorporating realistic noise models and hardware connectivity should sharpen the Pareto front even further.

In summary, GTQNNs offer a practical route toward quantum-enhanced machine learning on near-term devices by tightly coupling classical feature learning with quantum-native decision making and by explicitly optimising for the hardware constraints that dominate today's quantum landscape.

Declarations

Conflict of interest The author declares no competing interests.
Availability of data and materials The datasets used in paper are publicly available in the Python packages. The code will be available upon request.

References

[1] A. Abbas, D. Sutter, C. Zoufal, A. Lucchi, A. Figalli, and S. Woerner. The power of quantum neural networks. *Nature Computational Science*, 1(6):403–409, 2021. DOI: 10.1038/s43588-021-00084-1.

[2] M. Alam and S. Ghosh. DeepQMLP: A scalable quantum–classical hybrid deep neural network architecture for classification. In *Proc. 35th Int. Conf. VLSI Design & 21st Int. Conf. Embedded Systems (VLSID)*, pages 275–280. IEEE, 2022.

[3] H.-Y. Chen, Y.-J. Chang, S.-W. Liao, and C.-R. Chang. Deep Q-learning with hybrid quantum neural network on solving maze problems. Quantum Machine Intelligence, 2024, 6:2 https://doi.org/10.1007/s42484-023-00137-w

[4] C.-Y. Liu, E. J. Kuo, C. H. A. Lin *et al.* Training classical neural networks by quantum machine learning. 2024 IEEE International Conference on Quantum Computing and Engineering (QCE), 2024, Volume: 2, Pages: 34-38 DOI 10.1109/QCE60285.2024.10248 arXiv:2402.16465, 2024.

[5] I. MacCormack, C. Delaney, A. Galda, N. Aggarwal, and P. Narang. Branching quantum convolutional neural networks. *Physical Review Research*, 4(1):013117, 2022. DOI: 10.1103/PhysRevResearch.4.013117.

[6] J. Pointing. Do quantum neural networks have simplicity bias? *arXiv preprint* arXiv:2407.03266, 2024.

[7] M. Schuld. Supervised quantum machine learning models are kernel methods. *arXiv preprint* arXiv:2101.11020, 2021.

[8] S.-I. Amari. Natural gradient works efficiently in learning. *Neural computation*, 10(2):251–276, 1998. DOI: 10.1162/089976698300017746.

[9] F. Kunstner, P. Hennig, and L. Balles. Limitations of the empirical Fisher approximation for natural-gradient descent. In *Advances in Neural Information Processing Systems 32*, pages 4156–4167, 2019.

[10] B. R. Frieden. *Science from Fisher Information: A Unification*. Cambridge University Press, 2004. DOI: 10.1017/CBO9780511616907.

[11] J. J. Rissanen. Fisher information and stochastic complexity. *IEEE Transactions on Information Theory*, 42(1):40–47, 1996. DOI: 10.1109/18.481776.

[12] W. Ji, D. Liu, Y. Meng, and Y. Xue. A review of genetic-based evolutionary algorithms in SVM parameter optimisation. *Evolutionary Intelligence*, 14:1389–1414, 2021. DOI: 10.1007/s12065-020-00439-z.

[13] R. Lahoz-Beltra. Quantum genetic algorithms for computer scientists. *Computers*, 5(4):24, 2016. DOI: 10.3390/computers5040024.

[14] G. Acampora and A. Vitiello. Implementing evolutionary optimisation on actual quantum processors. *Information Sciences*, 575:542–562, 2021. https://doi.org/10.1016/j.ins.2021.06.049.

[15] S. Altares-López, A. Ribeiro, and J. J. García-Ripoll. Automatic design of quantum feature maps. *Quantum Science and Technology*, 6(4):045010, 2021. https://iopscience.iop.org/article/10.1088/2058-9565/ac1ab1.

[16] D. Chivilikhin, A. Samarin, V. Ulyantsev, I. Iorsh, A. R. Oganov, and O. Kyrienko. MoG-VQE: Multi-objective genetic variational quantum eigensolver. *arXiv preprint* arXiv:2007.04424, 2020.

[17] K. Deb, S. Agrawal, A. Pratap, and T. Meyarivan. A fast and elitist multiobjective genetic algorithm: NSGA-II. *IEEE Transactions on Evolutionary Computation*, 6(2):182–197, 2002. DOI: 10.1109/4235.996017.

[18] K. Miettinen. *Nonlinear Multiobjective Optimization*. Kluwer Academic Publishers, Boston, 1998.

[19] E.B. Alaia, I.H. Dridi, H. Bouchriha and P. Borne, *Genetic algorithm with pareto front selection for multi-criteria optimization of multi-depots and multi-vehicle pickup and delivery problems with time windows*, 2014 15th International Conference on Sciences and Techniques of Automatic Control and Computer Engineering, pp. 488-493, (2014).

[20] B. Barán, A. Carballude and M. Villagra, *Neighbor Optimization of N-Dimensional Quantum Circuits*, SN Computer Science 2, 2021

[21] M. Cerezo *et al.* Challenges and opportunities in quantum machine learning. *Nat. Comput. Sci.* **2**, 567 (2022).

[22] K. Beer *et al.* Training deep quantum neural networks. *Nat. Commun.* **11**, 808 (2020).

[23] V. Havlíček *et al.* Supervised learning with quantum-enhanced feature spaces. *Nature* **567**, 209–212 (2019).

[24] D. P. García, J. Cruz-Benito, F. J. García-Peñalvo. Systematic literature review: quantum machine learning and its applications. *Computer Science Review*: 51, 100619(2024).

[25] S. Sim, P. D. Johnson, A. Aspuru-Guzik. Expressibility and entangling capability of parameterized quantum circuits. *Adv. Quantum Technol.* **2**, 1900070 (2019).

[26] S. X. Zhang *et al.* TensorCircuit: a quantum software framework for the NISQ era. *Quantum* **7**, 912 (2023).

[27] E. Farhi, H. Neven. Classification with quantum neural networks on near-term processors. *arXiv*:1802.06002 (2018).

[28] K. Sharma *et al.* Trainability of dissipative perceptron-based quantum neural networks. *Phys. Rev. Lett.* **128**, 180505 (2022).

[29] A. Sagingalieva *et al.* Hybrid quantum neural network for drug response prediction. *Cancers* **15**, 2705 (2023).

[30] U. Singh, A. Z. Goldberg, K. Heshami. Coherent feed-forward quantum neural network. *Quantum Machine Intelligence* **6**, 89 (2024).

[31] M. Schuld. Supervised quantum machine learning models are kernel methods. *arXiv*:2101.11020 (2021).

[32] A. Vaswani *et al.* Attention is all you need. In *Advances in Neural Information Processing Systems 30*, pages 5998–6008, 2017.

[33] J. Devlin, M.-W. Chang, K. Lee, and K. Toutanova. BERT: Pre-training of deep bidirectional transformers for language understanding. In *Proceedings of NAACL*, pages 4171–4186, 2019. https://doi.org/10.18653/v1/N19-1423

[34] A. Dosovitskiy *et al.* An image is worth 16
*times*16 words: Transformers for image recognition at scale. *International Conference on Learning Representations*, 2021. https://arxiv.org/abs/2010.11929

[35] Jennewein, Douglas M. et al. The Sol Supercomputer at Arizona State University. PEARC '23: Practice and Experience in Advanced Research Computing 2023: Computing for the Common Good Pages 296 - 301, 2023. https://doi.org/10.1145/3569951.3597573

[36] H. Wang Several fitness functions and entanglement gates in quantum kernel generation. *Quantum Mach. Intell.*, 7, 7 (2025). https://doi.org/10.1007/s42484-024-00233-5

[37] H. Wang A novel feature selection method based on quantum support vector machine. *Physica Scripta*, 99 056006 (2024). , Volume 99, Number 5 https://doi.org/DOI 10.1088/1402-4896/ad36ef

[38] Antonio Benítez-Hidalgo, Antonio J. Nebro, José García-Nieto, Izaskun Oregi, Javier Del Ser, jMetalPy: A Python framework for multi-objective optimization with metaheuristics, *Swarm and Evolutionary Computation*, 51, 100598, 2019 https://doi.org/10.1016/j.swevo.2019.100598

[39] M. Schuld and F. Petruccione. *Machine Learning with Quantum Computers*. Springer International Publishing, Cham, 2021. https://link.springer.com/book/10.1007/978-3-030-83098-4.

[40] M. A. Nielsen and I. L. Chuang. *Quantum Computation and Quantum Information* (10th-anniv. ed.). Cambridge University Press, Cambridge, 2011.

[41] J. Biamonte, P. Wittek, N. Pancotti, P. Rebentrost, N. Wiebe, and S. Lloyd. Quantum machine learning. *Nature*, 549(7671):195–202, 2017. DOI: 10.1038/nature23474.

[42] M. Schuld, I. Sinayskiy, and F. Petruccione. An introduction to quantum machine learning. *Contemporary Physics*, 56(2):172–185, 2015. DOI: 10.1080/00107514.2014.964942.

[43] V. Havlíček, A. D. Córcoles, K. Temme *et al.* Supervised learning with quantum-enhanced feature spaces. *Nature*, 567(7747):209–212, 2019. DOI: 10.1038/s41586-019-0980-2.

[44] D. P. García, J. Cruz-Benito, and F. J. García-Peñalvo. Systematic literature review: Quantum machine learning and its applications. *arXiv:2201.04093*, 2022. DOI: 10.48550/arXiv.2201.04093.

[45] D. N. Diep. Some quantum neural networks. *International Journal of Theoretical Physics*, 59:1179–1190, 2020. DOI: 10.1007/s10773-020-04397-1.

[46] A. Chalumuri, R. Kune, and B. S. Manoj. A hybrid classical-quantum approach for multi-class classification. *Quantum Information Processing*, 20:119, 2021. DOI: 10.1007/s11128-021-03029-9.

[47] B. Q. Chen and X. F. Niu. Quantum Neural Network with Improved Quantum Learning Algorithm. *International Journal of Theoretical Physics*, 59:1978–1990, 2020. DOI: 10.1007/s10773-020-04470-9.

[48] F. Tacchino, S. Mangini, P. K. Barkoutsos *et al.* Variational Learning for Quantum Artificial Neural Networks. *IEEE Transactions on Quantum Engineering*, 2:1–10, 2021. DOI: 10.1109/TQE.2021.3062494.

[49] J. Wang, Y. Chen, R. Chakraborty, and S. X. Yu. Quantum gradient descent algorithms. *arXiv:1911.12207*, 2019. DOI: 10.48550/arXiv.1911.12207.

[50] Y. Li, R. G. Zhou, R. Xu, J. Luo, and W. Hu. A quantum deep convolutional neural network for image recognition. *Quantum Science and Technology*, 5:044003, 2020. DOI: 10.1088/2058-9565/ab9f93.

[51] S. L. Wu *et al.* Application of quantum ensemble learning to particle-physics analysis at the LHC. *Physical Review Research*, 3:033221, 2021. DOI: 10.1103/PhysRevResearch.3.033221.

[52] K. H. Wan, O. Dahlsten, H. Kristjánsson, R. Gardner, and M. S. Kim. Quantum generalisation of feed-forward neural networks. *npj Quantum Information*, 3:36, 2017. DOI: 10.1038/s41534-017-0032-4.

[53] K. Beer, D. Bondarenko, T. Farrelly *et al.* Training deep quantum neural networks. *Nature Communications*, 11:808, 2020. DOI: 10.1038/s41467-020-14454-2.

[54] I. Cong, S. Choi, and M. D. Lukin. Quantum convolutional neural networks. *Nature Physics*, 15:1273–1278, 2019. DOI: 10.1038/s41567-019-0648-8.

[55] K. Sharma, M. Cerezo, L. Cincio, and P. J. Coles. Trainability of dissipative perceptron-based quantum neural networks. *Physical Review Letters*, 128:180505, 2022. DOI: 10.1103/PhysRevLett.128.180505.

[56] M. G. Zhou, Z. P. Liu, H. L. Yin *et al.* Quantum Neural Network for Quantum Neural Computing. *Research*, 6:0134, 2023. DOI: 10.34133/research.0134.

[57] J. Preskill. Quantum computing in the NISQ era and beyond. *Quantum*, 2:79, 2018. DOI: 10.22331/q-2018-08-06-79.

[58] E. A. Cherrat, I. Kerenidis, N. Mathur, J. Landman, M. Strahm, and Y. Y. Li. Quantum vision transformers. *Quantum*, 8:1265, 2024. DOI: 10.22331/q-2024-02-22-1265.

[59] H. Ma, H. Shang, and J. Yang. Quantum embedding method with transformer neural network quantum states for strongly correlated materials. *npj Computational Materials*, 10:220, 2024. DOI: 10.1038/s41524-024-01406-3.

[60] H. Zhang and Q. Zhao. A survey of quantum transformers: Technical approaches, challenges and outlooks. *arXiv:2504.03192*, 2025. arXiv:2504.03192.

[61] Li, G., Zhao, X. , Wang, X. Quantum self-attention neural networks for text classification. Sci. China Inf. Sci. 67, 142501 (2024). https://doi.org/10.1007/s11432-023-3879-7

[62] A. Baevski, Y. Zhou, A. Mohamed, and M. Auli. wav2vec 2.0: A framework for self-supervised learning of speech representations. In *Advances in Neural Information Processing Systems 33*, pages 12449–12460, 2020. https://arxiv.org/abs/2006.11477

[63] E.B. Alaia, I.H. Dridi, H. Bouchriha and P. Borne, *Genetic algorithm with pareto front selection for multi-criteria optimization of multi-depots and multi-vehicle pickup and delivery problems with time windows*, 2014 15th International Conference on Sciences and Techniques of Automatic Control and Computer Engineering, pp. 488-493, (2014).